

## DYNAMICAL SIMULATION OF RED BLOOD CELL RHEOLOGY IN MICROVESSELS

TSORNG-WHAY PAN AND TONG WANG

*This paper is dedicated to Professor Roland Glowinski for his 70th birthday*

**Abstract.** A spring model is applied to simulate the skeleton structure of the red blood cell (RBC) membrane and to study the red blood cell (RBC) rheology in microvessels. The biconcave RBC shape in static plasma and tank-treading behavior of single cell in shear flows have been successfully captured in this model. The behavior of the RBC in a Poiseuille flow and the lateral migration of the cells in a shear flow have been investigated. It is found that the RBCs exhibit parachute shape in a Poiseuille flow with the curvature closely related to the deformability of the cell membrane and the hematocrit (Hct) of the blood. With this spring model, RBCs can recover their initial shapes associated with the minimal elastic energy when the flow stops. The simulation results also show that the RBCs migrate to the center of the domain in the radial direction in a shear flow, which clearly indicates the Fahraeus-Lindqvist effect in microvessels. The rate of migration toward the center depends on the shape of the RBC; the bioconcave shape enhances this migration.

**Key Words.** Computational Biomechanics, Microcirculation, Rheology, Red blood cells, Elastic membrane model, Immersed boundary method.

### 1. Introduction

The microcirculation, which is comprised of the microvessels of diameter smaller than  $100\mu m$ , is essential to the human body. It is where exchange of mass and energy takes place. At the microcirculatory level, the particulate nature of the blood becomes significant. The rheological property of the red blood cells (RBCs) is a key factor of the blood flow characteristics in microvessels because of their large volume fraction (40-45%), so called hematocrit (Hct), in the whole blood. Under normal conditions, RBCs are biconcave-shaped discs of about  $8\mu m$  in diameter. The cell membrane is highly deformable so that RBC can change its shape when an external force is acting on it and returns to the biconcave resting shape after the removal of the forces [13]. In microvessels having internal diameter close to the cell size,

---

Received by the editors October 30, 2008 and, in revised form, January 5, 2009.

2000 *Mathematics Subject Classification.* 65M60, 76M10, 76Z05.

The authors acknowledge the support of NSF (grants ECS-9527123, CTS-9873236, DMS-9973318, CCR-9902035, DMS-0209066, DMS-0443826).

the RBCs exhibit well known parachute shapes under flow [31]. In a bigger microvessel, RBCs tend to move across the streamlines of the flow, so called lateral migration, to the center of the vessel so that there is a cell-free layer near the vessel wall. The non-uniform distribution of hematocrit within the cross-section of the vessel is the physical reason of Fahraeus-Lindqvist effect [12] which is characterized by a decrease in the apparent blood viscosity in such microvessels.

As in [5], *in silico* mathematical modeling is an attractive alternative since it is difficult to deal with *in vivo* and *in vitro* experiments on studying microcirculation and RBC rheology due to the size limitation. Nowadays, numerical study of RBC rheology has attracted growing interest (see, e.g., [28]). For example, in [29] the parachute shape of RBCs in capillaries was investigated with different Hct and the apparent blood viscosity in capillaries was also studied by using the boundary-integral method with both Mooney-Rivlin and Skalak models plus bending resistance for the RBC membrane. In [11], an immersed boundary method was used to simulate 3D capsule and RBCs in shear flow with both neo-Hookean and Skalak models for membrane deformation. It was found that the bending resistance must be included in order to simulate complex shape of RBCs when they deform in shear flow. In [2], an immersed boundary method and a neo-Hookean model with and without bending resistance were used to simulate the interaction of two deformable cells in a shear flow in two dimensions. It was found that aggregates made of deformable cells are easily breakable by a shear flow, while those made of less deformable cells are not. In [20, 22], an immersed finite element method was presented for the simulation of RBCs in three dimensions while the RBC membrane employing a Mooney-Rivlin model. The microscopic mechanism of RBC aggregation has been linked to the macroscopic blood viscosity via direct numerical simulation and the relation between the effective viscosity of blood flow and the diameters of capillaries has been obtained. In [33], a semi-implicit particle method combined with a spring model was used to simulate a single file of RBCs between two parallel plates for various Hct in two dimensions. The parachute shape of RBCs in capillaries and flow resistance were investigated with different Hct. In [9], a discrete model for the RBC membrane has been constructed by taking into account the volume constraint of the RBC, the local area constraint on each triangle element from the mesh for the RBC membrane, the total area constraint of the RBC surface, the stretching force between nodes on each edge of the surface triangle element, and the preferred angle between triangle elements sharing a common edge (the bending resistance). These constraints give different forces acting on the nodes on the RBC surface. A lattice-Boltzmann method was combined with this discrete model to simulate 200 densely packed RBCs in three dimensional flow.

Among these methodologies and models mentioned above, we want to combine the immersed boundary method with spring model since we intend to simulate the mixture of deformable and rigid particles in microvessels in near future. We have already developed very efficient methodologies, called

distributed Lagrange multiplier/fictitious domain (DLM/FD) methods, for simulating rigid particles freely moving in Newtonian fluid in three dimensions [16, 17, 24]. The DLM/FD methods are closely related to the immersed boundary methods since they both use uniform grids on simple shape computational domain and the Lagrange multipliers play similar role as the force acting on the elastic membrane immersed in fluid for the immersed boundary methods. For modeling the RBC membrane, the general organization of the RBC membrane has been well characterized. The human RBC is a inflated closed membrane filled with a viscous fluid, called cytoplasm. The RBC membrane is a phospholipid bilayer plus the attached glycocalyx at the plasmatic face of the bilayer and a network of spectrins, called the cytoskeleton, fastened to the bilayer at its cytoplasmic face [13, 18]. The cytoskeleton is an elastic network which has triangular structure (and most of these triangles form hexagons) in the network (e.g., see [34]). This particular geometry, as well as the intrinsic elastic properties of the spectrin, allows the RBC to be highly deformable and elastic. Due to its special structure, the RBC membrane has strong resistance changes in area/volume and shear deformation [18]. Therefore, it is of significance to take into consideration the structure of the RBC membrane skeleton in the study of RBC rheology. Several spring models [8, 9, 10, 18, 30, 33] have been developed to illustrate the structure of the RBC membrane skeleton and to describe the deformability of the RBCs. In this article, the mechanical properties of the RBC membrane is predicted by a recently proposed elastic spring model which has been used in [33]. The simulation presented here is two-dimensional, and the methodology can be extended to three dimensions without difficulty.

In this article, we present computational simulation of the motion of deformable RBCs in microvessels. An immersed boundary method based on the Navier-Stokes equations is adapted for the fluid flow in a two dimensional channel. The present simulation uses a solution method incorporated with an operator splitting technique and finite element method with a fixed regular triangular mesh so faster solvers can be used for solving the fluid flow which is an important feature needed for simulating three dimensional flow involving deformable particles. The structure of this paper is as follows: We discuss the elastic spring model and numerical methods in Section 2. In Section 3, first we validate the model by reproducing the biconcave RBC in static plasma and tank-treading phenomenon of single RBC in shear flows and compare the results with the experimental data and existing numerical results. Then the shape behavior of RBCs in a Poiseuille flow and lateral migration in a shear flow are studied via numerical simulations. The conclusions are summarized in Section 4.

## 2. Models and methods

Let  $\Omega$  be a bounded rectangular domain filled with blood plasma which is incompressible, Newtonian, and contains RBCs with the viscosity of the cytoplasm same as that of the blood plasma. For some  $T > 0$ , the governing

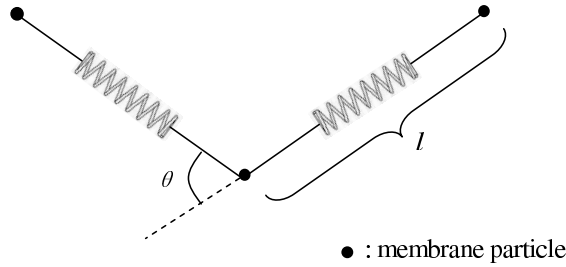


FIGURE 1. The elastic spring model of the RBC membrane

equations for the fluid-cell system are

$$(1) \quad \rho \left[ \frac{\partial \mathbf{u}}{\partial t} + (\mathbf{u} \cdot \nabla) \mathbf{u} \right] = -\nabla p + \mu \Delta \mathbf{u} + \mathbf{f} \text{ in } \Omega, \quad t \in (0, T),$$

$$(2) \quad \nabla \cdot \mathbf{u} = 0 \text{ in } \Omega, \quad t \in (0, T),$$

Equations (1) and (2) are completed by the following boundary and initial conditions:

$$(3) \quad \mathbf{u} = \mathbf{g} \text{ on the top and bottom of } \Omega \text{ and is periodic in the } x \text{ direction,}$$

$$(4) \quad \mathbf{u}(0) = \mathbf{u}_0.$$

where  $\mathbf{u}$  and  $p$  are the fluid velocity and pressure, respectively, anywhere in the flow,  $\rho$  is the fluid density, and  $\mu$  is the fluid viscosity, which is assumed to be constant for the entire fluid. In (1),  $\mathbf{f}$  is a body force which is the sum of  $\mathbf{f}_p$  and  $\mathbf{f}_B$  where  $\mathbf{f}_p$  is the pressure gradient pointing in the  $x$  direction when considering the cases of Poiseuille flow and  $\mathbf{f}_B$  accounts for the force acting on the fluid/cell interface.

**2.1. Elastic spring model for the RBC membrane.** The deformability and the elasticity of the RBC are due to the skeleton architecture of the membrane. A one-dimensional elastic spring model used in [33] is considered to describe the deformable behavior of the RBCs. Based on this model, the RBC membrane can be viewed as membrane particles connecting with the neighboring membrane particles by springs, as shown in Figure 1. Elastic energy stores in the spring due to the change of the length  $l$  of the spring with respect to its reference length  $l_0$  and the change in angle  $\theta$  between two neighboring springs. The total elastic energy of the RBC membrane,  $E = E_l + E_b$ , is the sum of the total elastic energy for stretch/compression and the total energy for bending which, in particular, are

$$(5) \quad E_l = \frac{k_l}{2} \sum_{i=1}^N \left( \frac{l_i - l_0}{l_0} \right)^2$$

and

$$(6) \quad E_b = \frac{k_b}{2} \sum_{i=1}^N \tan^2(\theta_i/2).$$

In equations (5) and (6),  $N$  is the total number of the spring elements, and  $k_l$  and  $k_b$  are spring constants for changes in length and bending angle, respectively. Based on the principle of virtual work, the elastic spring force acting on the  $i$ th membrane particle is then

$$(7) \quad \mathbf{F}_i = -\frac{\partial E}{\partial \mathbf{r}_i}$$

with  $\mathbf{r}_i$  the position of the  $i$ th membrane particle. In the simulation, this elastic force is a portion of the body force term in the Navier-Stokes equations.

**2.2. Immersed boundary method.** The immersed boundary method developed by Peskin, e.g, [25, 26, 27], is employed in this study because of its distinguish features in dealing with the problem of fluid flow interacting with a flexible fluid/structure interface. Over the years, it has demonstrated its capability in study of computational fluid dynamics including blood flow. Based on the method, the boundary of the deformable structure is discretized spatially into a set of boundary nodes. The force located at the immersed boundary node  $\mathbf{X}$  affects the nearby fluid mesh nodes  $\mathbf{x}$  through a 2D discrete  $\delta$ -function  $D_h(\mathbf{X} - \mathbf{x})$ :

$$(8) \quad \mathbf{F}(\mathbf{x}) = \sum \mathbf{F}(\mathbf{X})D_h(\mathbf{X} - \mathbf{x}) \quad \text{for } |\mathbf{X} - \mathbf{x}| \leq 2h,$$

where  $h$  is the uniform finite element mesh size and

$$(9) \quad D_h(\mathbf{X} - \mathbf{x}) = \delta_h(\mathbf{X}_1 - x_1)\delta_h(\mathbf{X}_2 - x_2)$$

with the 1D discrete  $\delta$ -functions being

$$(10) \quad \delta_h(z) = \begin{cases} \frac{1}{4h} \left(1 + \cos\left(\frac{\pi \cdot z}{2h}\right)\right) & \text{for } |z| \leq 2h, \\ 0 & \text{for } |z| > 2h. \end{cases}$$

The movement of the immersed boundary node  $\mathbf{X}$  is also affected by the surrounding fluid and therefore is enforced by summing the velocities at the nearby fluid mesh nodes  $\mathbf{x}$  weighted by the same discrete  $\delta$ -function:

$$(11) \quad \mathbf{U}(\mathbf{X}) = \sum h^2 \mathbf{u}(\mathbf{x})D_h(\mathbf{X} - \mathbf{x}) \quad \text{for } |\mathbf{X} - \mathbf{x}| \leq 2h.$$

After each time step, the position of the immersed boundary node is updated by

$$(12) \quad \mathbf{X}_{t+\Delta t} = \mathbf{X}_t + \Delta t \mathbf{U}(\mathbf{X}_t).$$

**2.3. Operator splitting technique.** We first apply the *Lie's scheme* [4, 16] to equations (1) and (2) with the backward Euler method in time for some subproblems and obtain the following fractional step subproblems:

$\mathbf{u}^0 = \mathbf{u}_0$  is given; for  $n \geq 0$ ,  $\mathbf{u}^n$  being known, solve

$$(13) \quad \begin{cases} \rho \frac{\mathbf{u}^{n+1/3} - \mathbf{u}^n}{\Delta t} + \nabla p^{n+1/3} = 0 \text{ in } \Omega, \\ \nabla \cdot \mathbf{u}^{n+1/3} = 0 \text{ in } \Omega, \\ \mathbf{u}^{n+1/3} = \mathbf{g}^{n+1} \text{ on the top and bottom of } \Omega \\ \text{and is periodic in the } x \text{ direction,} \end{cases}$$

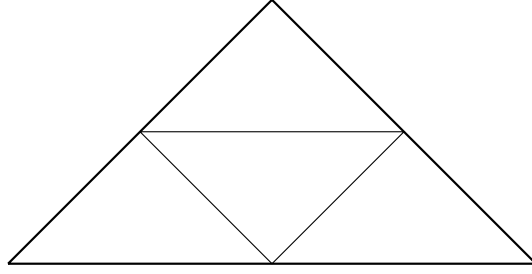


FIGURE 2. Schematic representation of a FEM triangulation and its subtriangulation.

Update the position of the membrane by (11) and (12) and then compute the force  $\mathbf{f}_B$  on the fluid/cell interface by (7) and (8). Now solve

$$(14) \quad \begin{cases} \frac{\partial \mathbf{u}(t)}{\partial t} + (\mathbf{u}^{n+1/3} \cdot \nabla) \mathbf{u}(t) = 0 & \text{in } \Omega \text{ on } (t^n, t^{n+1}), \\ \mathbf{u}(t^n) = \mathbf{u}^{n+1/3} & \text{in } \Omega, \\ \mathbf{u}(t) = \mathbf{g}^{n+1} & \text{on } \Gamma_-^{n+1} \times (t^n, t^{n+1}), \end{cases}$$

where  $\Gamma_-^{n+1} = \{\mathbf{x} | \mathbf{x} \in \Omega, \mathbf{g}^{n+1}(\mathbf{x}) \cdot \mathbf{n}(\mathbf{x}) < 0\}$ , and set  $\mathbf{u}^{n+2/3} = \mathbf{u}(t^{n+1})$ . Finally solve

$$(15) \quad \begin{cases} \rho \frac{\mathbf{u}^{n+1} - \mathbf{u}^{n+2/3}}{\Delta t} - \mu \Delta \mathbf{u}^{n+1} = \mathbf{f}^{n+1} & \text{in } \Omega, \\ \mathbf{u}^{n+1} = \mathbf{g}^{n+1} & \text{on the top and bottom of } \Omega \\ & \text{and is periodic in the } x \text{ direction.} \end{cases}$$

**2.4. Finite element approximation.** Subproblems (13)-(15) have been solved by finite element methods. Suppose that a rectangular computational domain  $\Omega \subset R^2$  is chosen with length  $\mathcal{L}$ ,  $h$  is a space discretization step,  $\mathcal{T}_h$  is a finite element triangulation of  $\bar{\Omega}$  for velocity, and  $\mathcal{T}_{2h}$  is a twice coarser triangulation for pressure (see Figure 2). Let  $P_1$  be the space of polynomials in two variables of degree  $\leq 1$ , we introduce the finite dimensional spaces:

$W_{g_h(t)} = \{\mathbf{v}_h | \mathbf{v}_h \in C^0(\bar{\Omega})^2, \mathbf{v}_h|_T \in (P_1)^2, \forall T \in \mathcal{T}_h, \mathbf{v}_h = \mathbf{g}_h(t) \text{ on the top and bottom of } \Omega \text{ and has period } \mathcal{L} \text{ in the } x \text{ direction}\},$

$W_{0h} = \{\mathbf{v}_h | \mathbf{v}_h \in C^0(\bar{\Omega})^2, \mathbf{v}_h|_T \in (P_1)^2, \forall T \in \mathcal{T}_h, \mathbf{v}_h = \mathbf{0} \text{ on the top and bottom of } \Omega \text{ and has period } \mathcal{L} \text{ in the } x \text{ direction}\},$

$L_h^2 = \{q_h | q_h \in C^0(\bar{\Omega}), q_h|_T \in P_1, \forall T \in \mathcal{T}_{2h} \text{ } q_h \text{ has period } \mathcal{L} \text{ in the } x \text{ direction}\}$

$L_{h,0}^2 = \{q_h | q_h \in L_h^2, \int_{\Omega} q_h d\mathbf{x} = 0\}.$

Then we have the following approximations of (13)-(15) (some of the subscripts  $h$  have been dropped):

$\mathbf{u}^0 = \mathbf{u}_{0h}$  is given; for  $n \geq 0$ ,  $\mathbf{u}^n$  being known, solve

$$(16) \quad \begin{cases} \rho \int_{\Omega} \frac{\mathbf{u}^{n+1/3} - \mathbf{u}^n}{\Delta t} \cdot \mathbf{v} d\mathbf{x} - \int_{\Omega} p^{n+1/3} (\nabla \cdot \mathbf{v}) d\mathbf{x} = 0, \quad \forall \mathbf{v} \in W_{0h}, \\ \int_{\Omega} q \nabla \cdot \mathbf{u}^{n+1/3} d\mathbf{x} = 0, \quad \forall q \in L_h^2, \\ \mathbf{u}^{n+1/3} \in W_{gh}^{n+1}, \quad p^{n+1/3} \in L_{h,0}^2. \end{cases}$$

Update the position of the membrane by (11) and (12) and then compute the force  $\mathbf{f}_B$  on the fluid/cell interface by (7) and (8). Now solve

$$(17) \quad \begin{cases} \int_{\Omega} \frac{\partial \mathbf{u}(t)}{\partial t} \cdot \mathbf{v} d\mathbf{x} + \int_{\Omega} (\mathbf{u}^{n+1/3} \cdot \nabla) \mathbf{u}(t) \cdot \mathbf{v} d\mathbf{x} = 0 \quad \text{on } (t^n, t^{n+1}), \\ \forall \mathbf{v} \in W_{0h}^{n+1,-}, \quad \mathbf{u}(t) \in W_h, \\ \mathbf{u}(t) = \mathbf{g}_h(t^{n+1}) \quad \text{on } \Gamma_-^{n+1} \times (t^n, t^{n+1}), \\ \mathbf{u}(t^n) = \mathbf{u}^{n+1/3}, \end{cases}$$

and set  $\mathbf{u}^{n+2/3} = \mathbf{u}(t^{n+1})$ . Finally solve

$$(18) \quad \begin{cases} \rho \int_{\Omega} \frac{\mathbf{u}^{n+1} - \mathbf{u}^{n+2/3}}{\Delta t} \cdot \mathbf{v} d\mathbf{x} + \mu \int_{\Omega} \nabla \mathbf{u}^{n+1} \cdot \nabla \mathbf{v} d\mathbf{x} = \int_{\Omega} \mathbf{f} \cdot \mathbf{v} d\mathbf{x}, \\ \forall \mathbf{v} \in W_{0h}, \quad \mathbf{u}^{n+1} \in W_{gh}^{n+1}. \end{cases}$$

In (16)-(18), we have  $W_{gh}^{n+1} = W_{gh(t^{n+1})}$ ,  $W_h = \{\mathbf{v}_h | \mathbf{v}_h \in C^0(\overline{\Omega})^2, \mathbf{v}_h|_T \in P_1 \times P_1, \forall T \in \mathcal{T}_h, \mathbf{v}_h \text{ is periodic in the } x \text{ direction with period } \mathcal{L}\}$ ,  $W_{0h}^{n+1,-} = \{\mathbf{v} | \mathbf{v} \in W_h, \mathbf{v} = \mathbf{0} \text{ on } \Gamma_-^{n+1}\}$ , and  $\mathbf{g}_h(t)$  is an approximation of  $\mathbf{g}(t)$  verifying  $\int_{\Gamma} \mathbf{g}_h(t) \cdot \mathbf{n} d\Gamma = 0$  where  $\Gamma$  is the top and bottom of  $\Omega$ .

The degenerated quasi-Stokes problem (16) is solved by a conjugate gradient method introduced in [16]. Equation (17) is an advection type subproblem. It is solved by a wave-like equation method, which is described in detail in [6], [7], and [23]. Problem (18) is a discrete elliptic system whose iterative or direct solution is a classical problem .

### 3. Numerical results and discussions

In this study, the RBCs are suspended in blood plasma which has a density  $\rho = 1.00g/cm^3$  and a dynamical viscosity  $\mu = 0.012g/(cm \cdot s)$ . The viscosity ratio which describes the viscosity contrast of the fluid inside and outside the RBC membrane is fixed at 1.0. The fluid domain is a two dimensional horizontal channel. For all computations, the grid resolution for the computational domain is 80 grid points per unit length with the unit length equal to  $10\mu m$  and the time step is  $\Delta t=0.001$  with the time unit equal to one millisecond. To obtain a Poiseuille flow, a constant pressure gradient is prescribed as a body force. To produce shear flow, a Couette flow driven by two walls at the top and bottom which have the same speed but move in directions opposite to each other is applied to the suspension. Different shear rate can be obtained by adjusting the wall speed. In addition, periodic conditions are imposed at the left and right boundary of the domain.

**3.1. Shape change of a swollen RBC.** In many cases of interest, the two-dimensional model approximates the shape of the RBC by the characteristic cross section in the plane that is parallel to the flow direction if the cell were in shear flow. In the following, the shape change of swollen RBC is simulated using the elastic spring model based on minimum energy principle as in [33]. Initially, the RBC is assumed to be a circle with a radius of  $2.8\mu m$ . The circle is discretized into  $N = 76$  membrane particles so that 76 springs are formed by connecting the neighboring particles. The shape change is stimulated by reducing the total area of the circle  $s_0$  through a penalty function

$$(19) \quad \Gamma_s = \frac{k_s}{2} \left( \frac{s - s_e}{s_e} \right)^2$$

and the total energy is modified as  $E + \Gamma_s$  and the force acting on the  $i$ th membrane particle now is

$$(20) \quad \mathbf{F}_i = - \frac{\partial(E + \Gamma_s)}{\partial \mathbf{r}_i}$$

where  $s$  and  $s_e$  are the time dependent area of the RBC and the equilibrium area of the RBC, respectively. When the area is reduced, each RBC membrane particle moves on the basis of the following equation of motion:

$$(21) \quad m\ddot{\mathbf{r}}_i + \gamma\dot{\mathbf{r}}_i = \mathbf{F}_i$$

Here,  $\dot{(\ )}$  denotes the time derivative;  $m$  and  $\gamma$  represent the membrane particle mass and the membrane viscosity of the RBC. The position  $\mathbf{r}_i$  of the  $i$ th membrane particle is solved by discretizing (21) via a second order finite difference method. The total energy stored in the membrane decreases as the time elapses. The final shape of the RBC shown in Figure 3 is obtained as the total elastic energy is minimized.

The parameters in the simulation of the shape change of the RBCs are set as follows: the membrane particle mass  $m$  is  $2.0 \times 10^{-4}g$  as in [33] and the membrane viscosity  $\gamma$  is  $8.8 \times 10^{-7}N \cdot s/m$  obtained in [21]. The bending constant was taken as  $k_b = 0.6 - 4.8 \times 10^{-12}N \cdot m$  in [33]. Here, the membrane parameters  $k_l$  and  $k_b$  are set to be in the range of  $0.01 - 3.0 \times 10^{-12}N \cdot m$  with  $k_l = k_b$  and the spring length can be kept almost constant with this choice of parameters (see Section 3.2). The penalty coefficient  $k_s$  in (19) is about  $k_b \times 10^4$ . The bending constant is closely related to the rigidity of the membrane. A higher  $k_b$  results a less deformable cell. Also when  $k_l$  is about 10 times smaller of  $k_b$  (at least for those  $k_b$  used in this article), the final shape is still circular. An initial circular shape is transformed into its final stable shape (see Figure 3) associated with a minimal energy for a given area ratio  $s^*$  regardless the choice of  $k_b$  in the above given range. It is found that when the reduced area  $s^* = s_e/s_0 \leq 0.8$ , biconcave shapes are obtained. When the ratio  $s^* > 0.8$ , the final stable shape is close to an ellipse. The biconcave shape obtained for  $s^* = 0.55$  resembles the normal physiological shape of the RBC very well.

After obtaining the shape of the RBC for a given reduced areas, such RBC shape is put into a  $20\mu m \times 20\mu m$  domain to obtain its equilibrium

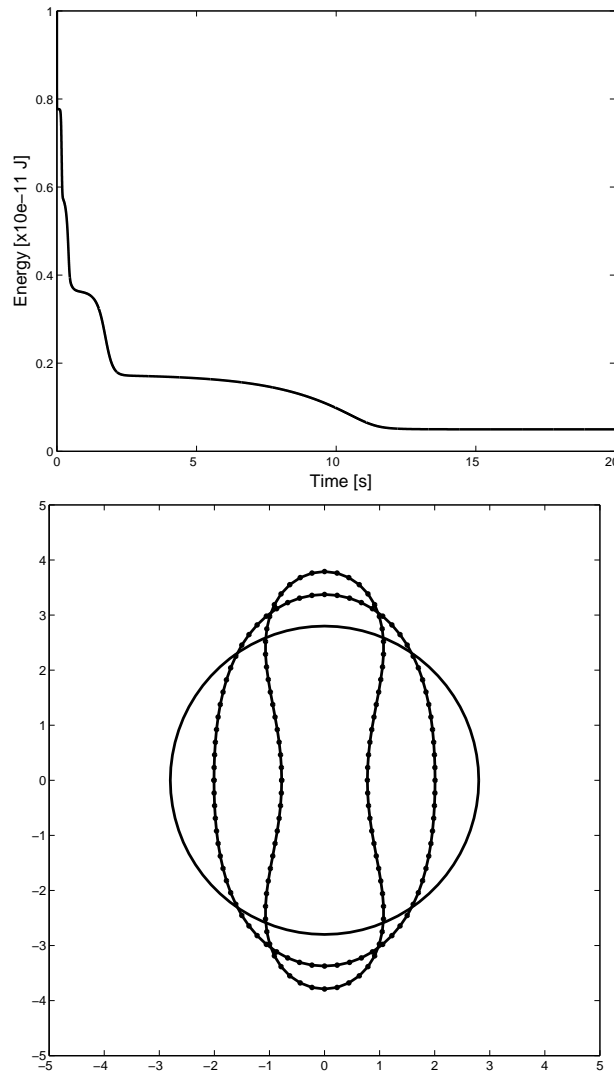


FIGURE 3. The top figure is an example of the history of the change in the elastic energy of RBC membrane with  $k_b = 3.0 \times 10^{-12} N \cdot m$ . The bottom one shows two dimensional RBC shapes obtained by reducing the area from a circle using the elastic model. Elliptic shape:  $s^* = 0.9$ ; biconcave shape:  $s^* = 0.55$ . Lines correspond to the RBC obtained from the elastic model while the dots show the equilibrium RBC shape in a static blood plasma.

shape in static plasma. For the results shown in this paper, the coupled RBC motion and fluid flow is solved by the immersed boundary method based on the Navier-Stokes equations with the force given (20) instead of the one in (7). The elastic force induced by the springs is substituted into the Navier-Stokes equations as a body force. The equilibrium shapes in

plasma shown in Figure 3 demonstrate that the RBCs simulated by elastic spring model are stable in blood plasma.

**3.2. Tank-treading in shear flows.** Tank-treading of RBC membrane in shear flow has been observed experimentally by Fischer *et al.* [14] and many others, e.g., [32]. It was observed that at equilibrium, although the global shape of the RBC is stationary, the membrane circulates along the contour like a tank tread with the cell orientating to a fixed inclination angle. It was also found that the tank-treading frequency was dependent on the shear rate and the viscosity of the surrounding viscous fluid [14]. We place the RBC obtained in static blood plasma with  $k_b$  in the range given in the previous section at the center in shear flow with dimension of  $20\mu m \times 20\mu m$ . Figure 4 shows the velocity fields for the biconcave and ellipse shaped RBCs when they are in a tank-treading motion in a shear flow of shear rate  $500 s^{-1}$ . In Figure 5, the elastic spring model is validated by comparing with previous experimental data [14], theoretical KS model [19], and simulations [3] for the inclination angles and tank-treading frequencies of RBC in shear flows. From Figure 5, we can see that our simulation results agree very well with those calculated by [3] for the inclination angles and with experimental data [14] for the tank-treading frequency. The small discrepancy between the simulation results and the theoretical prediction for the inclination angles may be due to the fact that the KS theory was based on the study of ellipsoidal shape instead of biconcave shape in [19]. We also keep track of the cell area and perimeter during the simulations. The change is less than  $\pm 0.1\%$  in the area and less than  $\pm 0.5\%$  in the perimeter.

**3.3. Shape behavior in a Poiseuille flow.** We now present the results of the simulation of shape behavior of RBCs in a Poiseuille flow through a narrow channel. The flow is from left to right. The pressure gradient is set as constant for this study so that the Reynolds number for the Poiseuille flow at the inlet is about 0.17 and the particle Reynolds numbers will be  $Re < 1$ . The cells studied are biconcave (resp., elliptical) shape with reduced area  $s^* = 0.55$  (resp.,  $s^* = 0.9$ ). The membrane constants are set to be  $5 \times 10^{-13} N \cdot m$  with  $k_l = k_b$ . In Figures 6 and 8, the fluid domain is  $20\mu m \times 10\mu m$  with single RBC placed in the center of the domain initially. Because of the periodic boundary condition at the inflow and outflow boundaries, this configuration corresponds to a hematocrit  $Hct=0.068$  (resp.,  $Hct=0.11$ ) for the biconcave RBC (resp., the ellipse RBC). In Figures 7 and 9, the fluid domain is  $10\mu m \times 10\mu m$  with two RBCs initially placed parallel to each other with center to center distance  $5\mu m$ . This configuration corresponds to a hematocrit  $Hct=0.27$  (resp.,  $Hct=0.44$ ) for the biconcave RBC (resp., the ellipse RBC). As shown in Figures 6 to 9 (from (a) to (d)), the well known parachute shape of RBCs has been observed for all the four cases. Moreover, the results demonstrated that the shape of the RBCs in a Poiseuille flow is closely related to the Hct of the blood. When the Hct is low, the cells are far from each other and the flow has the chance to develop after passing each cell. The cells are mainly influenced by the viscous force and the shape change

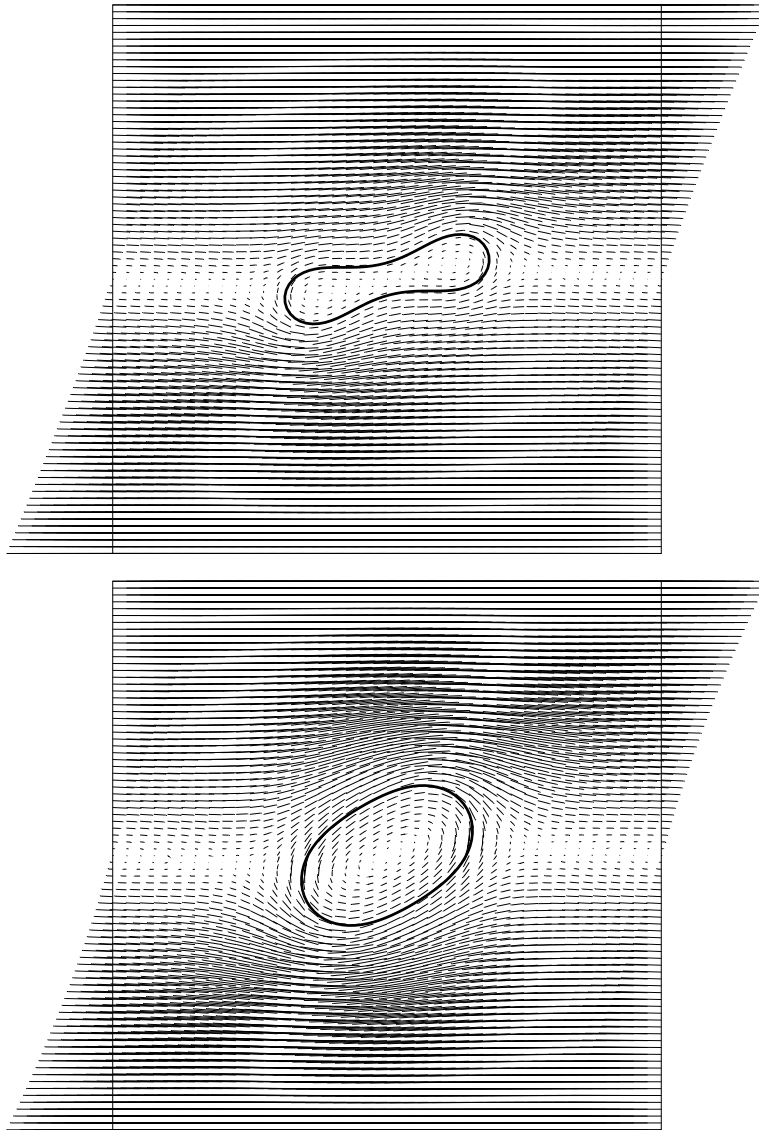


FIGURE 4. Velocity fields for the biconcave and ellipse shaped RBCs undergoing tank-treading motion in a shear flow of shear rate  $500 \text{ s}^{-1}$ .

is large (Figure 6 (a)-(d) and Figure 8 (a)-(d)). As the Hct increases, the flow is more blocked by the cells and the hydrodynamic interaction between adjacent cells also affect their motion; therefore the cells are less deformed (Figure 7 (a)-(d) and Figure 9 (a)-(d)). This result qualitatively agreed with those in [33].

We also study the ability of the cells returning back to initial shapes after stopping the flow. In Figures 6 to 9, the flow stops at  $t = 0.5 \text{ ms}$  and the results show that the deformed cells induced by flow are able to change back to their initial shapes as observed in [13]. Figure 10 shows the plot of the

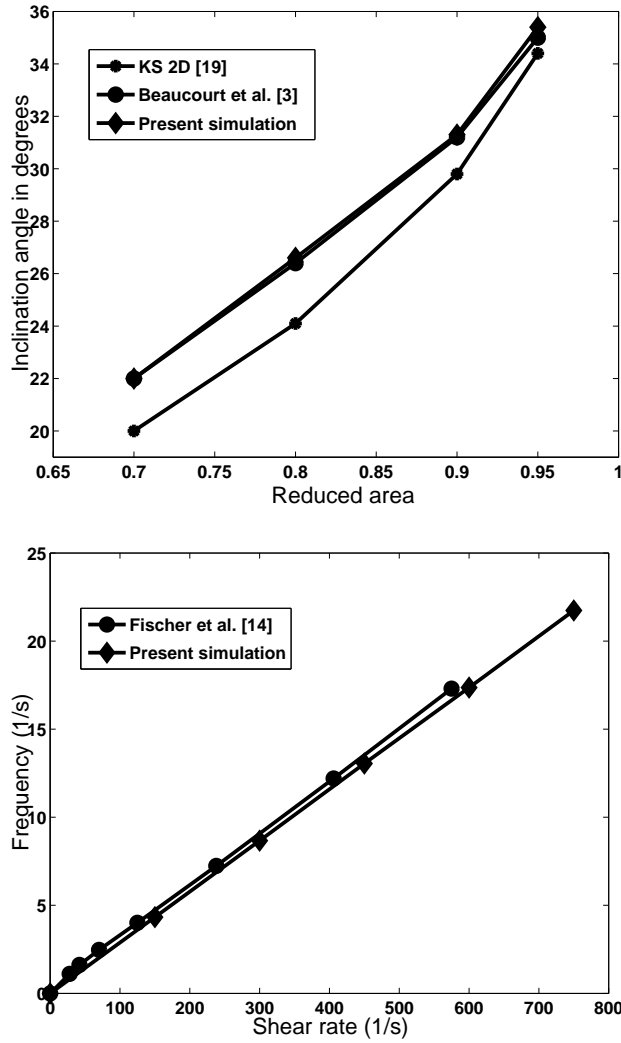


FIGURE 5. Equilibrium RBC inclination angle (top) as a function of reduced area  $s^*$ . Tank-treading frequency  $f$  (bottom) as a function of shear rate in a fluid with viscosity  $23cp$ .

total energy of the cell membrane versus time for the results of the biconcave cell shown in Figure 6. The increase in the total energy indicates the changes of the shape of the cell from a biconcave shape to a parachute shape under the flow and the total energy reaches a plateau when equilibrium is obtained. When the flow stops, the energy returns to the minimum as the cell quickly changes back to the initial biconcave shape. Similar energy behavior has been found for the other cases. In many other simulating results presented in literature, the biconcave shape is obtained from a description given in, e.g., [15] and the recovery of the biconcave shape has not been discussed.

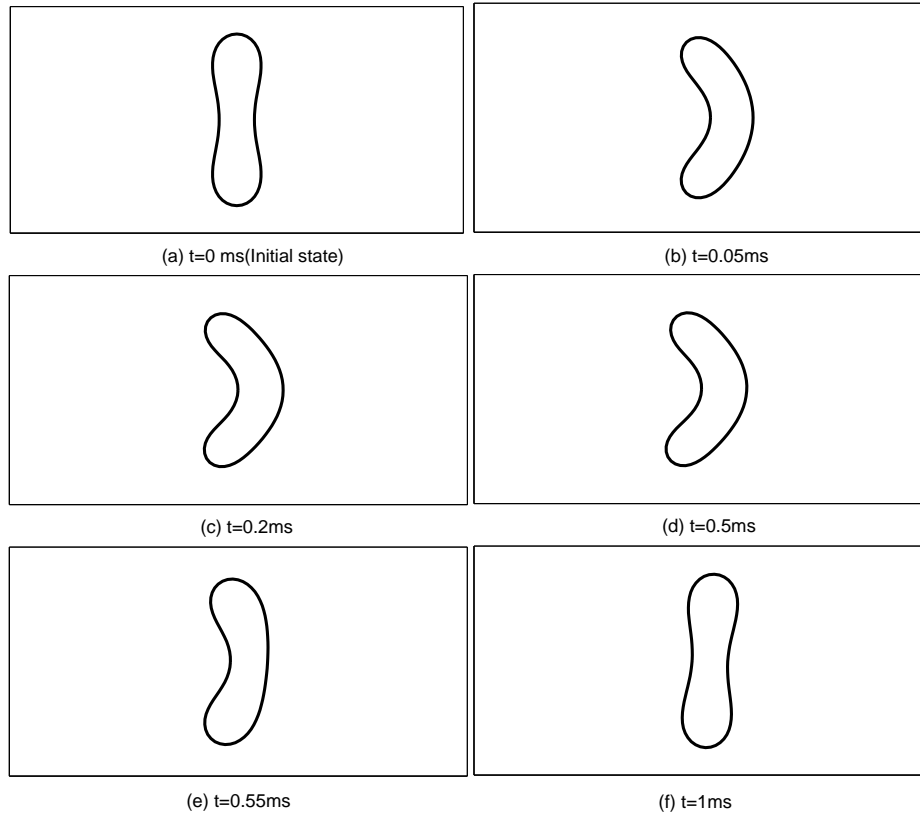


FIGURE 6. Snapshots of RBC behavior in a Poiseuille flow for the case of area ratio  $s^* = 0.55$  (Hct=0.068). The flow is from left to right and stops at  $t = 0.5ms$ .

**3.4. Lateral migration.** In this section, we describe the motion of a single, isolated RBC in shear flow with shear rate  $\gamma = 750s^{-1}$  in a rectangular domain of  $20\mu m \times 20\mu m$ . The shear flow is generated by moving the top wall to the left at a speed of  $7500\mu m/s$  and the bottom wall moving to the right at a same speed. Three different RBC shapes have been studied and the results are shown in Figure 11. All of them are with membrane constants  $k_l = k_b = 5 \times 10^{-13} N \cdot m$ . At time  $t = 0$ , the cells are located horizontally close to the bottom wall of the channel with a center to wall distance  $5\mu m$ . As the flow starts, the cells move longitudinally along the flow direction and laterally to the center of the domain with the shapes almost unchanged. For the biconcave and elliptical RBCs, the cell quickly oriented to a fixed angle as the flow starts. The inclination angles are stable for the entire computation and are the same as in the tank-treading case discussed in Section 3.2. It is also found that the migration velocity decreases with the increase of reduced area  $s^*$ . The biconcave RBC migrated to the center of the channel in 0.1 second; the elliptical RBC reached the center of the domain in 0.3 second, while it took more than 1 second for the almost circular RBC to move to

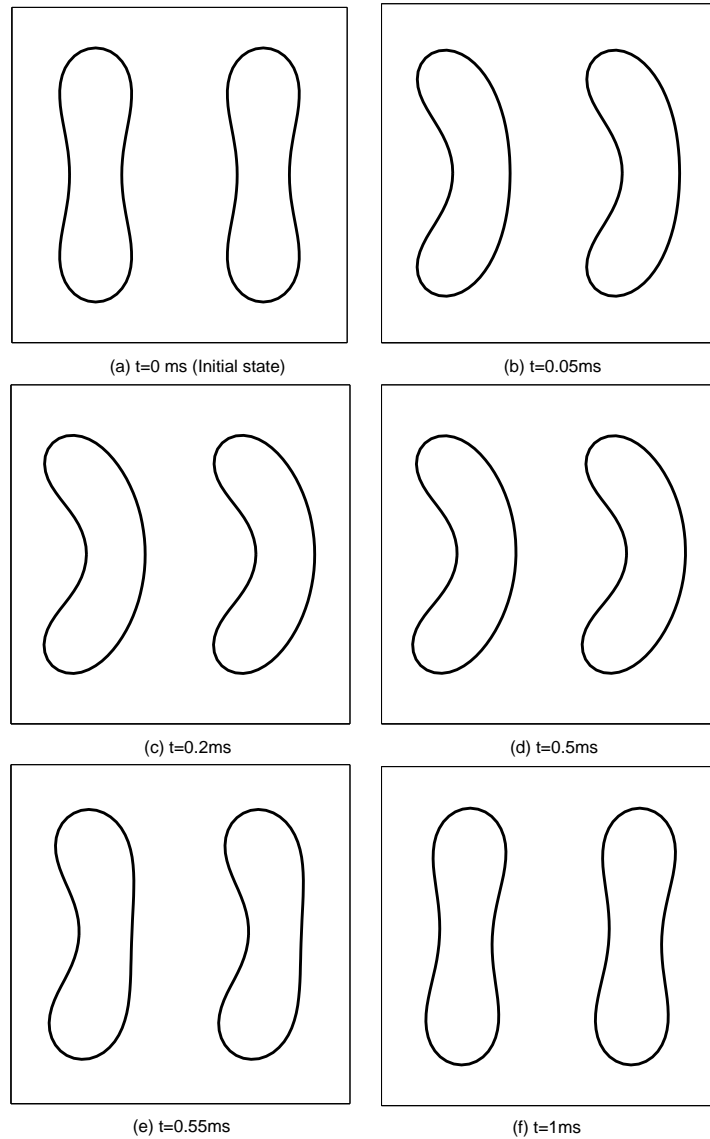


FIGURE 7. Snapshots of RBC behavior in a Poiseuille flow for the case of area ratio  $s^* = 0.55$  (Hct=0.27). The flow is from left to right and stops at  $t = 0.5$ ms.

the center in the same channel. This indicates that the lateral migration velocity is closely related to the shape of the RBCs and the biconcave shape enhances this migration. In [1] it was pointed out that the lateral migration velocity also depends on how easily the cell deforms; an easily deformable cell migrates faster toward the center of the vessel in a parabolic flow than a less deformable cell.

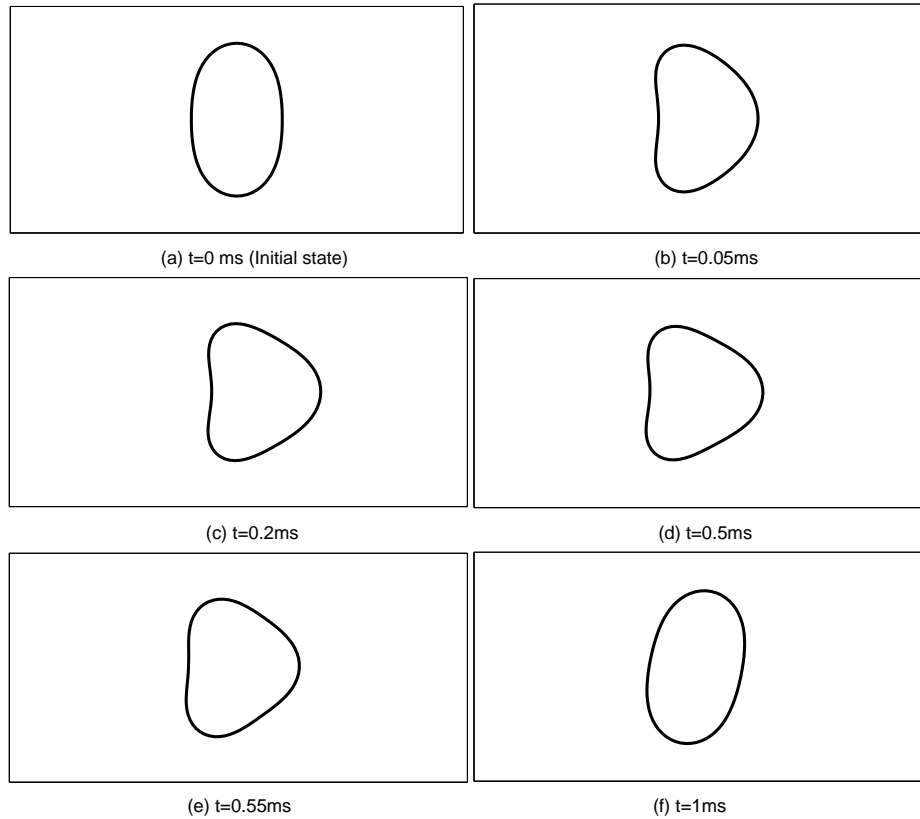


FIGURE 8. Snapshots of RBC behavior in a Poiseuille flow for the case of area ratio  $s^* = 0.9$  (Hct=0.11). The flow is from left to right and stops at  $t = 0.5ms$ .

#### 4. Conclusions

In summary, a numerical model is developed in this paper to investigate the rheology of RBCs in microvessels. Specifically, a novel elastic spring model is adopted to describe the cell membrane. Based on the available mechanical properties of RBCs, cells in Poiseuille flows and shear flows have been studied using a two-dimensional approximation. In a simple shear flow, tank-treading behavior of the cell membrane has been observed. The inclination angle and tank-treading frequency have been studied for various elastic constants and reduced areas. By comparing with the experimental data and other people's simulation results, it can be concluded that the elastic membrane model is capable of simulating the deformable property of the RBCs. In a Poiseuille flow of low Reynolds numbers, the RBCs in a narrow vessel deform themselves into parachute shapes. The steady shapes depend on the deformability of the membrane and the Hct of the blood. When the pressure gradient for generating the flow is taken off, the parachute shaped RBCs change back to the initial shapes that are obtained in static plasma, which shows the shape memory ability of the membrane describe

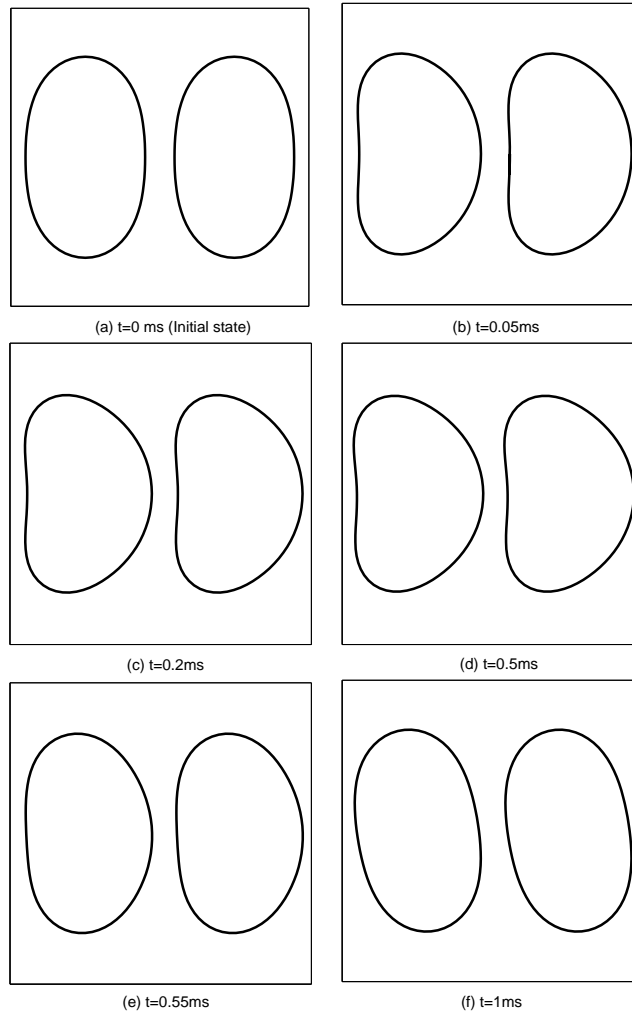


FIGURE 9. Snapshots of RBC behavior in a Poiseuille flow for the case of area ratio  $s^* = 0.9$  (Hct=0.44). The flow is from left to right and stops at  $t = 0.5ms$ .

by this model. Moreover, if a cell is placed asymmetrically with respect to the center in a shear flow, the cell migrates to the center with a fixed inclination angle as it drifts cross the streamline. The migration velocity is the fastest for the biconcave cells which shows that the RBCs tend to move to the center of the vessels, and thus a cell free layer can be formed. In addition, the numerical results are quantitatively/qualitatively similar to experimental observations and other investigators' findings showing that the potential of the numerical method described here for future studies of blood flow in microcirculation.

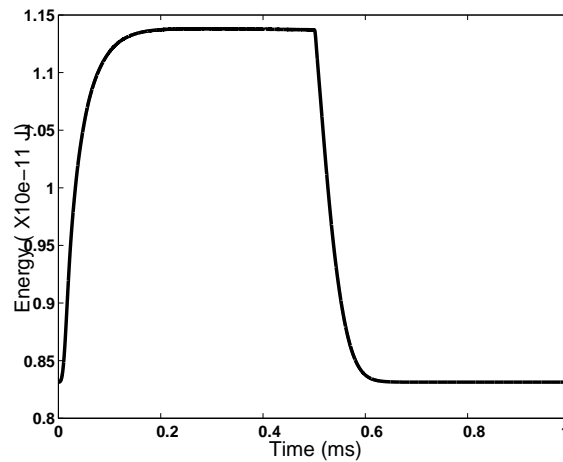


FIGURE 10. Example of the history of the change of elastic energy in a RBC membrane in a Poiseuille flow. The flow stops at  $t = 0.5ms$ .

### Acknowledgments

The authors acknowledge the support of NSF (grants ECS-9527123, CTS-9873236, DMS-9973318, CCR-9902035, DMS-0209066, DMS-0443826)

### References

- [1] P. Bagchi, Mesoscale simulation of blood flow in small vessels, *Biophys. J.*, 92 (2007) 1858-1877.
- [2] P. Bagchi, P. Johnson, A. Popel, Computational fluid dynamic simulation of aggregation of deformable cells in a shear flow, *J. Biomech. Eng.*, 127 (2005) 1070-1080.
- [3] J. Beaucourt, F. Rioual, T. Séon, T. Biben, C. Misbah, Steady to unsteady dynamics of a vesicle in a flow, *Phys. Rev. E*, 69 (2004) 011906.
- [4] A. J. Chorin, T. J. R. Hughes, M. F. McCracken, J. E. Marsden, Product formulas and numerical algorithms, *Comm. Pure Appl. Math.*, 31 (1978) 205-256.
- [5] V. Cristini V, G. S. Kassab, Computer modeling of red blood cell rheology in the microcirculation: a brief overview, *Ann. Biomed. Eng.*, 33 (2005) 1724-1727.
- [6] E.J. Dean, R. Glowinski, A wave equation approach to the numerical solution of the Navier-Stokes equations for incompressible viscous flow, *C. R. Acad. Sci. Paris, Série 1*, 325 (1997) 783-791.
- [7] E. J. Dean, R. Glowinski, T.-W. Pan, *A wave equation approach to the numerical simulation of incompressible viscous fluid flow modeled by the NavierStokes equations*. In *Mathematical and Numerical Aspects of Wave Propagation* (Ed. J. A. De Santo), p. 65-74, SIAM, Philadelphia, 1998.
- [8] C. Dubus, J.-B. Fournier, A Gaussian model for the membrane of red blood cells with cytoskeletal defects, *Europhys. Lett.*, 75 (2006) 181-187.
- [9] M. M. Dupin, I. Halliday, C. M. Care, L. Alboul, L. L. Munn, Modeling the flow of dense suspensions of deformable particles in three dimensions, *Phys. Rev. E*, 75 (2007) 066707.
- [10] W. Dzwinel, K. Boryczko, D. Yuen, A discrete-particle model of blood dynamics in capillary vessels, *J. Colloid Interface Sci.*, 258 (2003) 163173.
- [11] C. Eggleton, A. Popel, Large deformation of red blood cell ghosts in a simple shear flow, *Phys. Fluids*, 10 (1998) 1834-1845.

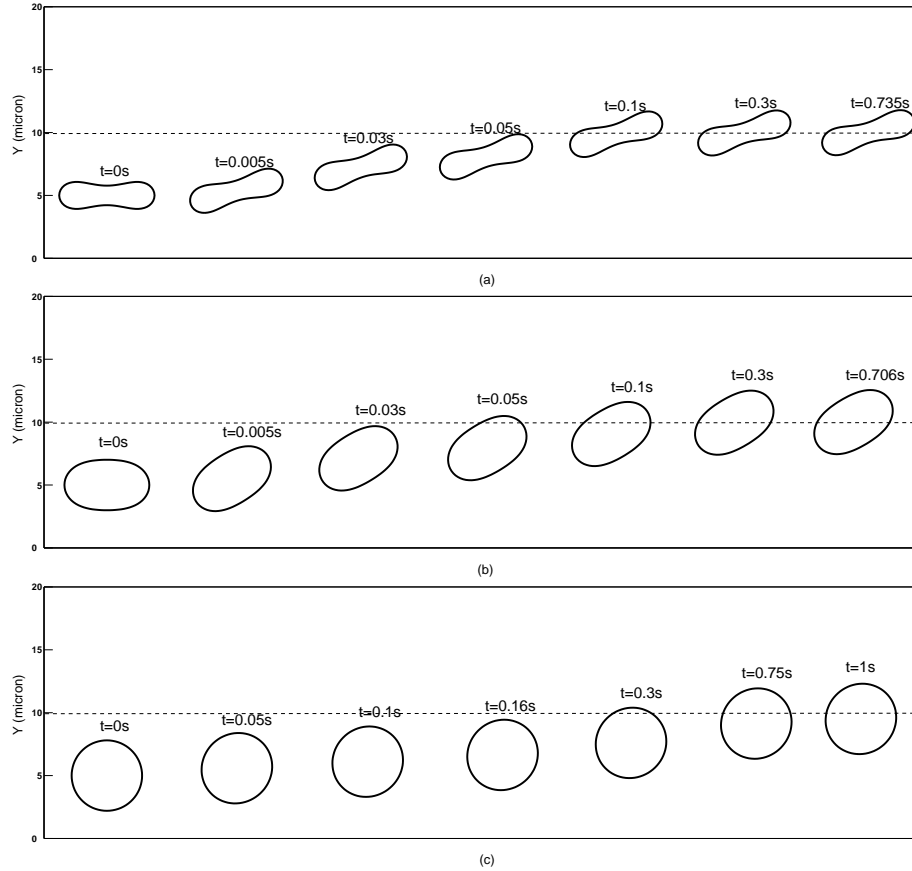


FIGURE 11. The lateral migration of RBCs in a shear flow with  $\gamma = 750s^{-1}$  for various  $s^*$ . The top wall moves to the left and the bottom wall to the right and the center of the vessel is shown by dashed line. (a)  $s^* = 0.55$ , (b)  $s^* = 0.9$ , (c)  $s^* = 1.0$ .

- [12] R. Fahraeus, T. Lindqvist, The viscosity of blood in narrow capillary tubes, *Am. J. of Physiol.*, 96 (1931) 562-568.
- [13] T. M. Fischer, Shape memory of human red blood cells, *Biophys. J.*, 86 (2004) 3304-3313.
- [14] T. M. Fischer, M. Stöhr-Liesen, H. Schmid-Schönbein, The red cell as a fluid droplet: tank tread-like motion of the human erythrocyte membrane in shear flow, *Science*, 202 (1978) 894-896.
- [15] Y. C. Fung, *Biomechanics: Mechanical Properties of Living Tissues*, Springer-Verlag, New York, 1993.
- [16] R. Glowinski, *Finite element methods for incompressible viscous flow*. In *Handbook of Numerical Analysis* (Eds. P.G. Ciarlet and J.-L. Lions), Vol.IX, p 3-1176, North-Holland, Amsterdam, 2003.
- [17] R. Glowinski, T.-W. Pan, T. I. Hesla, D.D. Joseph, J. Periaux, A fictitious domain approach to the direct numerical simulation of incompressible viscous flow past moving rigid bodies: Application to particulate flow, *J. Comput. Phys.*, 169 (2001) 363-427.

- [18] J. C. Hansen, S. Skalak, A. Hoger, An elastic network model based on the structure of the red blood cell membrane skeleton, *Biophys. J.*, 70 (1996) 146-166.
- [19] S. R. Keller, R. Skalak, Motion of a tank-treading ellipsoidal particle in a shear flow, *J. Fluid Mech.*, 120 (1982) 27-47.
- [20] W. K. Liu, Y. Liu, D. Farrell, L. Zhang, X. S. Wang, Y. Fukui, N. Patankar, Y. Zhang, C. Bajaj, J. Lee, J. Hong, X. Chen, H. Hsu, Immersed finite element method and its applications to biological systems, *Comput. Methods Appl. Mech. Eng.*, 195 (2006) 1722-1749.
- [21] X. Liu, Z.-Y. Tang, Z. Zeng, X. Chen, W.-J. Yao, Z.-Y. Yan, Y. Shi, H.-x. Shan, D.-G. Sun, D.-Q. He, Z.-Y. Wen, The measurement of shear modulus and membrane surface viscosity of RBC membrane with Ektacytometry: A new technique, *Math. Biosci.*, 209 (2007) 190-204.
- [22] Y. Liu, W. K. Liu, Rheology of red blood cell aggregation by computer simulation, *J. Comput. Phys.*, 220 (2006) 139-154.
- [23] T.-W. Pan, R. Glowinski, A projection/wave-like equation method for the numerical simulation of incompressible viscous fluid flow modeled by the Navier-Stokes equations, *Computational Fluid Dynamics Journal*, 9 (2000) 28-42.
- [24] T.-W. Pan, D. D. Joseph, R. Bai, R. Glowinski, V. Sarin, Fluidization of 1204 spheres: simulation and experiments, *J. Fluid Mech.*, 451 (2002) 169-191.
- [25] C. S. Peskin, Numerical analysis of blood flow in the heart, *J. Comput. Phys.*, 25 (1977) 220-252.
- [26] C. S. Peskin, The immersed boundary method, *Acta Numer.*, 11 (2002) 479-517.
- [27] C. S. Peskin, D. M. McQueen, Modeling prosthetic heart valves for numerical analysis of blood flow in the heart, *J. Comput. Phys.*, 37 (1980) 11332.
- [28] C. Pozrikidis, *Modeling and Simulation of Capsules and Biological Cells*, Chapman & Hall/CRC, Boca Raton, 2003.
- [29] C. Pozrikidis, Axisymmetric motion of a file of red blood cells through capillaries, *Phys. Fluids*, 17 (2005) 031503.
- [30] T. W. Secomb, B. Styp-Rekowska, A. R. Pries, Two-dimensional simulation of red blood cell deformation and lateral migration in microvessels, *Ann. Biomed. Eng.*, 35 (2007) 755-765.
- [31] R. Skalak, P. I. Branemark, Deformation of red blood cells in capillaries, *Science*, 164 (1969) 717-719.
- [32] R. Tran-Son-Tay, S. P. Suter, P. R. Rao, Determination of red blood cell membrane viscosity from rheoscopic observations of tank-treading motion, *Biophys. J.*, 46 (1984) 65-72.
- [33] K. Tsubota, S. Wada, T. Yamaguchi, Simulation study on effects of hematocrit on blood flow properties using particle method, *J. Biomech. Sci. Eng.*, 1 (2006) 159-170.
- [34] C. Vera, R. Skelton, F. Bossens, L. A. Sung, 3-D nanomechanics of an erythrocyte junctional complex in equibiaxial and anisotropic deformations, *Ann. Biomed. Eng.*, 33 (2005) 1387-1404.

Department of Mathematics, University of Houston, Houston, Texas 77204-3008, USA  
*E-mail:* pan@math.uh.edu and twang@math.uh.edu  
*URL:* <http://www.math.uh.edu/~pan/>